RESEARCH ARTICLE | OCTOBER 04 2024

Electric field sensitivity of molecular color centers

Kathleen R. Mullin; James M. Rondinelli

Appl. Phys. Lett. 125, 144004 (2024)
https://doi.org/10.1063/5.0217753

Applied Physics Letters ARTICLE pubs.aip.org/aip/apl

Electric field sensitivity of molecular color centers

Cite as: Appl. Phys. Lett. **125**, 144004 (2024); doi: 10.1063/5.0217753
Submitted: 6 May 2024 · Accepted: 19 September 2024 ·
Published Online: 4 October 2024

Kathleen R. Mullin and James M. Rondinelli[a)]

AFFILIATIONS

Department of Materials Science and Engineering, Northwestern University, Evanston, Illinois 60208, USA

[a)]Author to whom correspondence should be addressed: jrondinelli@northwestern.edu

ABSTRACT

Molecular color centers with $S = 1$ ground states are promising candidates for quantum sensing of electric fields. These molecules have an electronic structure similar to solid state color centers, but they allow for processing modalities that permit direct interfacing with an analyte. Currently, it is unknown how sensitive these molecules are to electric fields and what molecular properties affect their sensitivity. We perform density functional theory calculations to understand the impact of electric fields on the electronic structure of five nominally tetrahedral molecular color centers exhibiting variable transition metal chemistry and ligand densities. We then extract the Stark parameters from each of these molecules and compare them to molecular properties such as the dipole moment and inner shell stiffness and find that the dipole moment of the molecule largely governs sensitivity. We predict that polar heteroleptic molecules may have electric field sensitivities comparable to solid state color centers such as nitrogen-vacancy centers in diamond.

Molecular color centers (MCCs), recently discovered optically addressable electric spin molecular qubits, show promise as a quantum sensing platform. These molecules have been demonstrated to be addressable with ODMR (optically detected magnetic resonance) and EPR (electron paramagnetic resonance) and to have properties that can be synthetically tailored.[1,2] Molecular color centers are named after solid state color centers, as they share similar electronic structures. Both molecular and solid state color centers have an $S = 1$, triplet ground state, an $S = 0$, singlet excited state, and have a first excited state energy within the optical spectrum allowing for them to be initialized and read out with ODMR.[3,4]

Electric field sensitivity of MCCs arises from a Stark effect, whereby spectral field lines are split when exposed to an electric field. This splitting impacts both the ground state zero field splitting as well as the excited state energy, usually measured experimentally as the zero phonon line.[5] This leads to two possible modalities for sensing. All optical sensing, wherein an electric field couples to an optical transition, and spin-electron sensing, wherein an electric field couples to a spin transition. The Stark effect describes the change in energy (ΔE) of these states to the applied electric field ($\mathcal{E}_i$), applied in direction i, where the change is due to linear coupling, $\Delta\mu$, from a dipolar contribution and quadratic coupling, $\Delta\alpha$, from the polarizability, with the $\mathcal{E}$ field as

$$\Delta E_i = -\Delta\mu_i\mathcal{E}_i - \frac{1}{2}\Delta\alpha_i\mathcal{E}_i^2 \ . \quad (1)$$

Electric field sensing has been demonstrated using both organic molecules and solid state color centers by utilizing the Stark effect. Fluorescent, dibenzoterrylene (DBT) has been shown to have a large Stark parameter of 15 GHzm/MV in all optical electric field sensing experiments.[6] Electric field sensing has been demonstrated using solid state color centers by utilizing the Stark effect.[5] Anionic diamond nitrogen vacancy (NV) centers and neutral divacancies (V_C, V_S) in silicon carbide have both been used to sense electric fields with sensitivities of 6.6 and 10 GHzm/MV, respectively.[7,8] These materials host defects with a polar C_{3v} structure yielding large linear changes and a corresponding large $\Delta\mu$ parameter that allows for effective sensing of electric fields.[9–11] Other solid state color centers have been explored, including tin vacancy centers in diamond, where a nonpolar D_{3d} defect leads to a quadratic change in energy with applied field.[12]

MCCs, while currently experimentally unstudied as quantum electric field sensors, would operate as sensors using the same principles as solid state color centers. Although both point defects in a bulk structure and molecules are zero dimensional, molecules can be more controllably embedded in a flexible matrix for the creation of thin films that directly interface the molecule with an analyte. Synthetic chemistry allows the structure and chemistry of these MCCs to be precisely tuned, tailoring both properties, like spin relaxation times that are critical for qubit initialization and readout and sensitivity to external fields.[1]

Here, we perform density functional theory (DFT) to understand the electric field sensitivity of a family of 4-coordinate, near tetrahedral, $S = 1$ molecules. We examine how variations in ligands, metal cation, and symmetry impact the sensitivity to electric field (Fig. 1). One of the included molecules is an experimentally known optically addressable molecular qubit Cr(*o*-tolyl)$_4$.[3] Cr(norbornyl)$_4$ and Mo(*o*-tolyl)$_4$ are both experimentally known electron paramagnetic resonance (EPR) addressable qubits, but only Cr(norbornyl)$_4$, also referred to as Cr(nor)$_4$, is optically active.[13] The remaining two qubits, Cr(*o*-tolyl)$_3$Me and Cr(*o*-tolyl)$_3$Me-F, have not been synthesized, but are heteroleptic molecules similar to Cr(*o*-tolyl)$_4$. We examine how changes to the rigidity and polarity of the molecules affect the Stark parameters, calculated via changes to the first excited state energy under electric fields of different magnitudes. We find that the dipole moment and rigidity of the metal ligand bonds largely govern the electric field sensitivity of the molecule. The results suggest the MCCs can be more sensitive to electric fields if they include heavier transition metals or larger dipole moments.

In addition to contributing to changes in electronic structure that lead to different degrees of experimental addressability, the different metal-ligand interactions in these molecules lead to an array of inner shell metal-ligand bond lengths (Table I). These molecules also include a range of symmetries. Most of the molecules exhibit polar point groups, with Cr(*o*-tolyl)$_4$, Cr(*o*-tolyl)$_3$Me, and Cr(*o*-tolyl)$_3$Me-F sharing the C_1 symmetry and Cr(norbornyl)$_4$) having C_{2v} symmetry. We use the C_1 Cr(*o*-tolyl)$_4$ structure, which matches the experimentally determined point group for pure Cr(*o*-tolyl)$_4$.[14] The only nonpolar molecule studied, Mo(*o*-tolyl)$_4$, has the S_4 point group. These changes in point group and ligands also lead to an array of dipole moments (Table I) defined in a coordinate system as shown in Fig. 1(a).

Our DFT calculations were performed using Vienna *Ab initio* Simulation Package[15–18] with projector augmented wave potentials[19,20] (VASP version 6.3.2) and the PBE exchange correlation functional.[21,22] We used a 600 eV energy cutoff for the plane wave expansion with a total energy convergence of 1×10^{-9} eV, and the following valence configurations: Cr($3d^5 4s^1$), C($2s^2 2p^2$), F($2s^2 2p^5$), H($1s^1$), and Mo ($4d^5 4s^1$). All calculations were performed on isolated molecules in a simulation cell providing a spacing of 15 Å between periodic images of the molecule in all directions. Γ-point calculations were performed with Gaussian smearing of 0.05 eV for the Brillouin zone integrations. All components of the system were initially relaxed with a force convergence of 10^{-3} meV Å^{-1}. Dipole moment calculations were performed with respect to the center of mass of each molecule.

TABLE I. Bond lengths (Å) and dipole moments μ (in units of Debye).

Molecule	Symmetry	Average M-C Bond length	μ_x	μ_y	μ_z
Cr(*o*-tolyl)$_4$	C_1	1.99	0.043	0.027	0.008
Mo(*o*-tolyl)$_4$	S_4	2.08	0	0	0
Cr(norbornyl)$_4$	C_{2v}	2.02	0.002	0.002	0.001
Cr(*o*-tolyl)$_3$Me	C_1	1.98	0.459	0.012	0.194
Cr(*o*-tolyl)$_3$Me-F	C_1	1.98	0.456	1.421	0.750

Excited state (*es*) calculations were performed using the ΔSCF method,[23,24] which has been shown to reliably calculate Stark parameters for solid state color centers.[25] We calculated the spin flip excited state energy ($E_{es}^{\uparrow\downarrow}$) by subtracting the total energy of a constrained occupancy calculation, where the electron occupying the spin-up HOMO is promoted to the spin-down LUMO, from a standard ground state DFT calculation. For all calculations, including the constrained occupancy calculations, the relaxed ground state geometry is used. Changes in the $E_{es}^{\uparrow\downarrow}$ were then used to calculate the Stark parameters by fitting the changes in energy to Eq. (1).

Local stiffness calculations were performed via finite displacements of the central metal atoms inside the ligand cages using a method similar to that employed by Amdur *et al.*[26] The potential energy is calculated as $U = U_0 + \frac{1}{2}(\Delta\mathbf{r})^T\mathbf{H}(\Delta\mathbf{r})$, where U_0 is the reference potential energy, $\Delta\mathbf{r}$ is the finite displacement vector from the equilibrium position, and $\mathbf{H}$ is the matrix of the second order polynomial terms approximating the Hessian. Finite displacements were evaluated on a $5 \times 5 \times 5$ grid about the equilibrium position in increments of 0.01 Å.

We first calculated the ground state electronic structure on all five molecules in the absence of an electric field. All molecules have a HOMO and LUMOs with majority *d* character shown via the color map projected on to the orbital diagram, Fig. 2. Mo(*o*-tolyl)$_4$ shows more *p*-*d* hybridization in the spin-up HOMO and the spin-up and spin-down LUMOs compared to the other molecules. Cr(nor)$_4$ has the largest HOMO-LUMO gaps of 2.38 and 2.51 eV for $E_{gs}^{\uparrow\uparrow}$ and $E_{gs}^{\uparrow\downarrow}$, respectively, followed by Cr(*o*-tolyl)$_4$ and Mo(*o*-tolyl)$_4$ with 1.52 eV

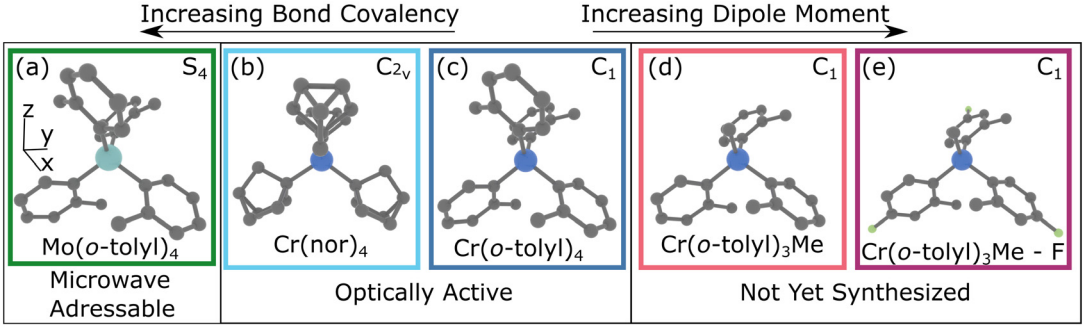

FIG. 1. Visualization of known (a) microwave addressable molecules, (b) and (c) optically addressable molecules, and (d) and (e) not yet synthesized molecules. Arrows above the molecules indicate changes of interest to the ground state properties. The axes in (a) represent the consistent frame of reference used for all five molecules.

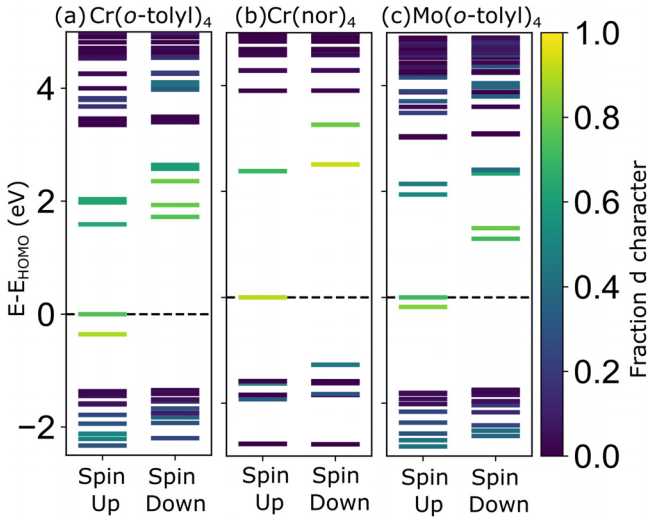

FIG. 2. Quantitative molecular orbital diagrams highlighting the d-orbital character of (a) Cr(o-tolyl)$_4$, (b) Cr(nor)$_4$, and (c) Mo(o-tolyl)$_4$.

(1.64 eV) and 1.94 eV (1.1 eV) for $E_{gs}^{\uparrow\uparrow}$ ($E_{gs}^{\uparrow\downarrow}$). Cr(*o*-tolyl)$_3$Me and Cr(*o*-tolyl)$_3$Me-F have very similar gaps to Cr(*o*-tolyl)$_4$ with 1.80 eV (1.60 eV) and 1.77 eV (1.62 eV), respectively. $E_{es}^{\uparrow\downarrow}$ for all molecules follow the same trend in values as $E_{gs}^{\uparrow\downarrow}$, with energies of 0.54, 0.60, and 0.32 eV for Cr(*o*-tolyl)$_4$, Cr(nor)$_4$, and Mo(*o*-tolyl)$_4$, respectively. Cr(*o*-tolyl)$_3$Me has the same $E_{gs}^{\uparrow\downarrow}$ value of 0.53 regardless of fluorination. The *d* character of the HOMO and LUMO correlate with the excited state energy values, with Cr(nor)$_4$ showing the largest *d* character and Mo(*o*-tolyl)$_4$ showing the smallest. Visualization of the spin up HOMO and spin down LUMO can be found in the SI.

Next, we relaxed each molecule under applied electric fields between 0.5 and 7.5 MV/cm along the *x* and *z* directions. For each electric field direction and magnitude, we calculated $E_{es}^{\uparrow\downarrow}$ [Figs. 3(a) and 3(b)]. We found a range of responses for the molecules, with Cr(*o*-tolyl)$_4$ showing the smallest change in $E_{es}^{\uparrow\downarrow}$ of −0.21 meV for a maximum electric field of 7.5 MV/cm applied along *x*. Cr(*o*-tolyl)$_3$Me-F showed the largest change of −9.6 meV for a maximum electric field of 7.5 MV/cm applied along *z*.

Equation (1) was used to extract Stark parameters from $E_{es}^{\uparrow\downarrow}$ and are presented in Fig. 4. The change in dipole moment Stark parameter, $\Delta\mu$, is very small for all but the heteroleptic molecules, Cr(*o*-tolyl)$_3$Me and Cr(*o*-tolyl)$_3$Me-F. As $\Delta\mu$ is the linear Stark parameter, this increase is also reflected in the change in the linearity of $\Delta E_{es}^{\uparrow\downarrow}$ with electric field for the heteroleptic molecules, shown in Fig. 3. This trend contrasts with that of the change in polarizability Stark parameter, $\Delta\alpha$, which is very small for all molecules except Mo(*o*-tolyl)$_4$ and Cr(nor)$_4$. For these molecules, increased quadratic character is seen in $\Delta E_{es}^{\uparrow\downarrow}$ with electric field in Fig. 3.

In order to better understand why the Stark parameters vary across this series of molecules, we use two descriptors, the inner shell stiffness (κ) and the dipole moment (μ). The former quantity describes how strongly the metal center is bound within the ligand cage, with higher values indicating stiffer bonds. We find that κ is largest for Mo(*o*-tolyl)$_4$ and smallest for Cr(*o*-tolyl)$_4$ [Fig. 4(d)]. The trend between $\Delta\alpha$ and κ suggests that less tightly bound metal centers are more polarizable, which leads to larger quadratic change in $E_{es}^{\uparrow\downarrow}$ with applied electric field.

Additionally, we calculated the dipole moments for each of the molecules and found that $\Delta\mu$ trends positively with the magnitude of the dipole moment, indicating that more polar molecules should have stronger linear responses to the electric field [Fig. 4(b)]. Although our result is consistent with experimental studies of color centers in solids, which show that nonpolar color centers exhibit quadratic responses, we find that the most important factor contributing to the electric field response is the magnitude of the dipole moment. This differs from the

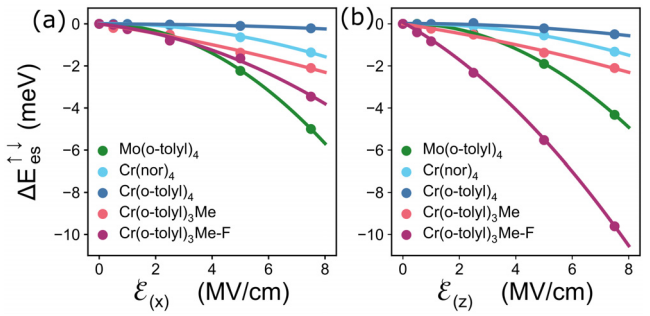

FIG. 3. Change in $E_{es}^{\uparrow\downarrow}$ with electric fields applied along the (a) *x* and (b) *z* axis.

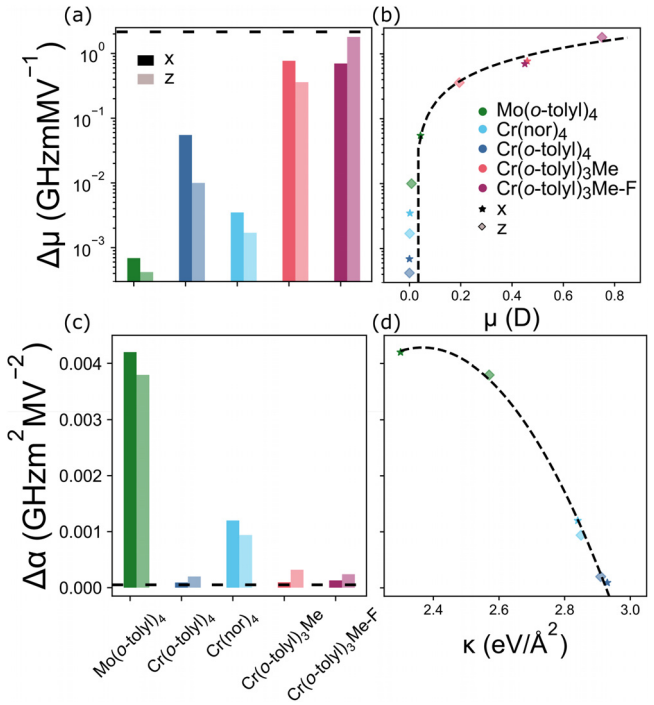

FIG. 4. Calculated Stark parameters, $\Delta\mu$ (a) and $\Delta\alpha$ (c), for the *x* and *z* directions for all studied molecules. Dotted lines in (a) and (c) indicate literature Stark parameters for the diamond NV center[5] and the Sn vacancy center,[12] respectively. Variation in (b) $\Delta\mu$ with μ and (d) $\Delta\alpha$ with κ for all molecules. κ is equivalent for Cr(*o*-tolyl)$_4$ and its homoleptic variants. Dashed lines are a linear fit for (b) and a quadratic fit for (d).

experimental emphasis placed on the point group of the color center controlling the electric field coupling parameter.[5,12]

Additional work is needed for MCCs to be used in devices as sensors. One possible applications of these molecules is to sense electric fields from two dimensional ferroelectrics, such as In_2Se_3[27,28] and $MoTe_2$,[29] in which switchable polarization has been demonstrated in few-layer samples. Current electrometry tools, such as piezoelectric force microscopy and its local hysteresis measurements, are used to perform such measurements. It is often challenging to assess if these materials are ferroelectric, because the local-probe measurements are difficult to perform and can suffer from artifacts arising from extrinsic electrostatic contributions.[30] New tools are needed to more accurately map electric fields from these materials. MCCs, like those presented here, present a potential solution. As with solid state color centers, coupling these molecular crystals to a photonic cavity may allow for enhanced emissions and more precise sensing.[31–34]

For MCCs to be employed as sensors for 2D ferroelectrics, they will need to be diluted in a diamagnetic material and processed into thin films to be interfaced with the analyte. Molecules in these films at far distances from the analyte will behave similarly to isolated molecules, with only the additional impacts from the chosen matrix. In the near and intermediate ranges to the analyte, the properties of the MCCs will be influenced by nonelectric field interactions with the surface. The impact will primarily be steric changes to the molecular structure, which will impact the zero phonon line even with no external electric field. A challenge with using these molecules as sensors for electric fields near the surface of the analyte will be separating physical, chemical, and electric field contributions to changes in the magnetic sublevels of the MCC. These impacts will likely vary with the thickness of the molecular film, decreasing with increasing sensor-analyte distance until the point that they represent a negligible, smaller than resolution, contribution to the change in energy. Another consideration is how the host matrix will affect the symmetry of the molecule once it is embedded. Experiments have shown that the symmetry of the molecule can change and could have a sizeable effect on the Stark parameters. Future studies are needed to understand how electrical, chemical, and mechanical interactions from proximity to the surface affect the molecule. Tunable responses or differential experiments may be needed to appropriately calibrate the sensors and determine sensitivity. Another factor to consider when experimentally utilizing these molecules is the optical linewidth of the various transitions. For use in sensing, molecules will need narrow optical linewidths, typically <500 MHz,[35] so future work should focus on understanding the effects of the molecule's chemistry and structure on optical linewidth.

In summary, we found that small electric fields quadratically change the excited state energy of molecules with small dipole moments. Such fields cause a linear change in the excited state energy of molecules with large dipole moments. Although a polar molecule is required for the linear Stark effect to be observed, a polar point group without a large dipole exhibits a quadratic response to an electric field. We find that decreased metal-ligand rigidity leads to a larger change in the quadratic Stark parameter, $\Delta\alpha$, while increased dipole moments lead to larger changes in the linear, $\Delta\mu$, response. These molecules are shown to be attractive candidates for electric field sensors particularly when nanoscale interfacing with the analyte is necessary. Further work is needed to optimize the electric field coupling parameter of the molecules and understand how the sensitivity changes when interfaced with analytes.

See the supplementary material for visualizations of the HOMO and LUMO levels.

We thank Professor Danna Freedman, Dr. Daniel Laorenza, and David Ullery for insightful discussions. This work was supported by the U.S. Department of Energy, Office of Science, Basic Energy Sciences under Award DE-SC0019356. This work used resources at the National Energy Research Scientific Computing Center, a DOE Office of Science User Facility, supported by the Office of Science of the U.S. Department of Energy under Contract No. DE-AC02-05CH11231 using NERSC award BES-ERCAP0023827.

AUTHOR DECLARATIONS

Conflict of Interest

The authors have no conflicts to disclose.

Author Contributions

Kathleen R. Mullin: Conceptualization (equal); Formal analysis (lead); Investigation (lead); Methodology (lead); Visualization (equal); Writing – original draft (lead). **James M. Rondinelli:** Conceptualization (equal); Funding acquisition (lead); Project administration (lead); Supervision (lead); Writing – review & editing (equal).

DATA AVAILABILITY

The data that support the findings of this study are available from the corresponding author upon reasonable request.

REFERENCES

[1]D. W. Laorenza, A. Kairalapova, S. L. Bayliss, T. Goldzak, S. M. Greene, L. R. Weiss, P. Deb, P. J. Mintun, K. A. Collins, D. D. Awschalom, T. C. Berkelbach, and D. E. Freedman, "Tunable Cr^{4+} molecular color centers," J. Am. Chem. Soc. **143**, 21350–21363 (2021).

[2]S. L. Bayliss, P. Deb, D. W. Laorenza, M. Onizhuk, G. Galli, D. E. Freedman, and D. D. Awschalom, "Enhancing spin coherence in optically addressable molecular qubits through host-matrix control," Phys. Rev. X **12**, 031028 (2022).

[3]S. L. Bayliss, D. W. Laorenza, P. J. Mintun, B. D. Kovos, D. E. Freedman, and D. D. Awschalom, "Optically addressable molecular spins for quantum information processing," Science **370**, 1309–1312 (2020).

[4]Y. Shen, T. M. Sweeney, and H. Wang, "Zero-phonon linewidth of single nitrogen vacancy centers in diamond nanocrystals," Phys. Rev. B **77**, 033201 (2008).

[5]P. Tamarat, T. Gaebel, J. R. Rabeau, M. Khan, A. D. Greentree, H. Wilson, L. C. L. Hollenberg, S. Prawer, P. Hemmer, F. Jelezko, and J. Wrachtrup, "Stark shift control of single optical centers in diamond," Phys. Rev. Lett. **97**, 083002 (2006).

[6]A. Moradi, Z. Ristanović, M. Orrit, I. Deperasińska, and B. Kozankiewicz, "Matrix-induced linear stark effect of single dibenzoterrylene molecules in 2,3-dibromonaphthalene crystal," ChemPhysChem **20**, 55–61 (2019).

[7]P. Tamarat, N. B. Manson, J. P. Harrison, R. L. McMurtrie, A. Nizovtsev, C. Santori, R. G. Beausoleil, P. Neumann, T. Gaebel, F. Jelezko, P. Hemmer, and J. Wrachtrup, "Spin-flip and spin-conserving optical transitions of the nitrogen-vacancy centre in diamond," New J. Phys. **10**, 045004 (2008).

[8]C. F. de las Casas, D. J. Christle, J. Ul Hassan, T. Ohshima, N. T. Son, and D. D. Awschalom, "Stark tuning and electrical charge state control of single divacancies in silicon carbide," Appl. Phys. Lett. **111**, 262403 (2017).

[9]M. Hollendonner, S. Sharma, S. K. Parthasarathy, D. B. R. Dasari, A. Finkler, S. V. Kusminskiy, and R. Nagy, "Quantum sensing of electric field distributions

of liquid electrolytes with NV-centers in nanodiamonds," New J. Phys. **25**, 093008 (2023).
[10]W. S. Huxter, M. F. Sarott, M. Trassin, and C. L. Degen, "Imaging ferroelectric domains with a single-spin scanning quantum sensor," Nat. Phys. **19**, 644–648 (2023).
[11]Z. Qiu, A. Hamo, U. Vool, T. X. Zhou, and A. Yacoby, "Nanoscale electric field imaging with an ambient scanning quantum sensor microscope," npj Quantum Inf. **8**, 1–7 (2022).
[12]L. De Santis, M. E. Trusheim, K. C. Chen, and D. R. Englund, "Investigation of the stark effect on a centrosymmetric quantum emitter in diamond," Phys. Rev. Lett. **127**, 147402 (2021).
[13]D. W. Laorenza, K. R. Mullin, L. R. Weiss, S. L. Bayliss, P. Deb, D. D. Awschalom, J. M. Rondinelli, and D. E. Freedman, "Coherent spin-control of $S = 1$ vanadium and molybdenum complexes," Chem. Sci. **15**, 14016–14026 (2024).
[14]S. U. Koschmieder, B. S. McGilligan, G. McDermott, J. Arnold, G. Wilkinson, B. Hussain-Bates, and M. B. Hursthouse, "Aryl and aryne complexes of chromium, molybdenum, and tungsten. x-ray crystal structures of [Cr(2-MeC$_6$H$_4$)(μ-2-MeC$_6$H$_4$)(PMe$_3$)]$_2$, Mo(η^2-2-MeC$_6$H$_3$)(2-MeC$_6$H$_4$)$_2$(PMe$_2$Ph)$_2$, and W(η^2-2,5-Me$_2$C$_6$H$_2$)(2,5-Me$_2$C$_6$H$_3$)$_2$-(PMe$_3$)$_2$," J. Chem. Soc., Dalton Trans. **1990**, 3427–3433.
[15]G. Kresse and J. Hafner, "*Ab initio* molecular dynamics for liquid metals," Phys. Rev. B **47**, 558–561 (1993).
[16]G. Kresse and J. Hafner, "*Ab initio* molecular-dynamics simulation of the liquid-metal–amorphous-semiconductor transition in germanium," Phys. Rev. B **49**, 14251–14269 (1994).
[17]G. Kresse and J. Furthmüller, "Efficiency of ab-initio total energy calculations for metals and semiconductors using a plane-wave basis set," Comput. Mater. Sci. **6**, 15–50 (1996).
[18]G. Kresse and J. Furthmüller, "Efficient iterative schemes for *ab initio* total-energy calculations using a plane-wave basis set," Phys. Rev. B **54**, 11169–11186 (1996).
[19]G. Kresse and D. Joubert, "From ultrasoft pseudopotentials to the projector augmented-wave method," Phys. Rev. B **59**, 1758–1775 (1999).
[20]P. E. Blöchl, "Projector augmented-wave method," Phys. Rev. B **50**, 17953–17979 (1994).
[21]J. P. Perdew, K. Burke, and M. Ernzerhof, "Generalized gradient approximation made simple [Phys. Rev. Lett. 77, 3865 (1996)]," Phys. Rev. Lett. **78**, 1396–1396 (1997).
[22]J. P. Perdew, K. Burke, and M. Ernzerhof, "Generalized gradient approximation made simple," Phys. Rev. Lett. **77**, 3865–3868 (1996).
[23]A. Hellman, B. Razaznejad, and B. I. Lundqvist, "Potential-energy surfaces for excited states in extended systems," J. Chem. Phys. **120**, 4593–4602 (2004).
[24]J. Gavnholt, T. Olsen, M. Engelund, and J. Schiøtz, "Δ self-consistent field method to obtain potential energy surfaces of excited molecules on surfaces," Phys. Rev. B **78**, 075441 (2008).
[25]L. Alaerts, Y. Xiong, S. Griffin, and G. Hautier, "A first principles study of the Stark shift effect on the zero-phonon line of the NV center in diamond," arXiv:2403.07771 (2024).
[26]M. J. Amdur, K. R. Mullin, M. J. Waters, D. Puggioni, M. K. Wojnar, M. Gu, L. Sun, P. H. Oyala, J. M. Rondinelli, and D. E. Freedman, "Chemical control of spin–lattice relaxation to discover a room temperature molecular qubit," Chem. Sci. **13**, 7034–7045 (2022).
[27]W. Ding, J. Zhu, Z. Wang, Y. Gao, D. Xiao, Y. Gu, Z. Zhang, and W. Zhu, "Prediction of intrinsic two-dimensional ferroelectrics in In_2Se_3 and other III_2-VI_3 van der Waals materials," Nat. Commun. **8**, 14956 (2017).
[28]Y. Zhou, D. Wu, Y. Zhu, Y. Cho, Q. He, X. Yang, K. Herrera, Z. Chu, Y. Han, M. C. Downer, H. Peng, and K. Lai, "Out-of-plane piezoelectricity and ferroelectricity in layered α-In_2Se_3 nanoflakes," Nano Lett. **17**, 5508–5513 (2017).
[29]S. Yuan, X. Luo, H. L. Chan, C. Xiao, Y. Dai, M. Xie, and J. Hao, "Room-temperature ferroelectricity in $MoTe_2$ down to the atomic monolayer limit," Nat. Commun. **10**, 1775 (2019).
[30]R. K. Vasudevan, N. Balke, P. Maksymovych, S. Jesse, and S. V. Kalinin, "Ferroelectric or non-ferroelectric: Why so many materials exhibit "ferroelectricity" on the nanoscale," Appl. Phys. Rev. **4**, 021302 (2017).
[31]B. Kim, H. Kurokawa, K. Sakai, K. Koshino, H. Kosaka, and M. Nomura, "Diamond optomechanical cavity with a color center for coherent microwave-to-optical quantum interfaces," Phys. Rev. Appl. **20**, 044037 (2023).
[32]G. Calusine, A. Politi, and D. D. Awschalom, "Cavity-enhanced measurements of defect spins in silicon carbide," Phys. Rev. Appl. **6**, 014019 (2016).
[33]D. O. Bracher, X. Zhang, and E. L. Hu, "Selective Purcell enhancement of two closely linked zero-phonon transitions of a silicon carbide color center," Proc. Natl. Acad. Sci. U. S. A. **114**, 4060–4065 (2017).
[34]G. Calusine, A. Politi, and D. D. Awschalom, "Silicon carbide photonic crystal cavities with integrated color centers," Appl. Phys. Lett. **105**, 011123 (2014).
[35]S. B. van Dam, M. Walsh, M. J. Degen, E. Bersin, S. L. Mouradian, A. Galiullin, M. Ruf, M. IJspeert, T. H. Taminiau, R. Hanson, and D. R. Englund, "Optical coherence of diamond nitrogen-vacancy centers formed by ion implantation and annealing," Phys. Rev. B **99**, 161203 (2019).